Available online at www.sciencedirect.com

SciVerse ScienceDirect

Journal of the European Ceramic Society 32 (2012) 569–577

www.elsevier.com/locate/jeurceramsoc

Design and processing of ZnO doped tricalcium phosphate based materials: Influence of β/α polymorph phase assemblage on microstructural evolution

L. Carbajal *, A. Caballero, M.A. Sainz

Ceramic Department, Instituto de Cerámica y Vidrio, CSIC, 28045 Madrid, Spain

Received 7 June 2011; received in revised form 21 September 2011; accepted 26 September 2011
Available online 20 October 2011

Abstract

Tricalcium phosphate (TCP) based biomaterials are excellent candidates in hard tissue engineering due to their similarity to the natural bone composition and outstanding properties. The presence of additives such as (Mg^{2+}, Zn^{2+}, F^{-}, CO_3^{2-} and/or SiO_4^{-}) in solid solution in the structure of TCP, affects the stability of its different polymorphs and therefore the properties of TCP based biomaterials. It is known that the incorporation of zinc in TCP in the non-toxic level stimulates bone growth and its mineralization, hence its interest. Nevertheless its effect on phase assemblage and microstructure evolution has not been clearly established. The main purpose of this study was to synthesize TCP and zinc doped monophasic/biphasic α/β-TCP dense biomaterials, by solid-state sintering process, with different ZnO contents and controlled phase proportions and microstructure on the final material. The effect of ZnO content and sintering temperature on phase assemblage, densification and microstructural evolution has been investigated.

Keywords: (A) Powders-solid state reaction; (B) Microstructure-final; (B) Tricalcium phosphate; (D) ZnO; (E) Biomedical applications

1. Introduction

The development of complete analog human bone tissue materials able to replace the mineral component is one of our major challenges nowadays. As the inorganic part of the bone is composed principally of Ca and P, there is an extensive use of calcium–phosphate-based biomaterials[1–4] in medical applications, for hard tissue replacement such as bone and tooth implants. The most widely used calcium phosphate based bioceramics are hydroxyapatite ($Ca_{10}(PO_4)_6(OH)_2$ – HAp) and tricalcium phosphate ($Ca_3(PO_4)_2$ – TCP). In the case of TCP its extensive use is related to its excellent biocompatibility, bioresorbability and osteoconductivity.

TCP has three polymorphs β, α and α′ in order of increasing temperature being only β and α the stable/metastable phases at room temperature. One of the main drawbacks within the use of TCP based biomaterials is related to the high dissolution rate and degradation of α-TCP ($K_{sp} = 10^{-25.5}$) and β-TCP ($K_{sp} = 10^{-29.5}$) when compared to HAp ($K_{sp} = 10^{-58.6}$) at 37 °C.[5] TCP based bioceramics[4,6] are expected to degrade in the host and be gradually replaced by the regenerating bone, meanwhile they act as a seed for the new bone and a supplier of Ca^{2+} and PO_4^{3-} ions. At early time, the degradation of β-TCP based materials is mild and stimulates bone formation, whereas at longer time its rapid dissolution may disturb the activity of host cells and generate adverse effects on bone tissues.[7,8] This high solubility of β-TCP decreases the bone implant strength and therefore the "*in vivo*" experiments are extremely dependent on the rate of dissolution and how it can be chemically modified. On the other hand, HAp based materials are stable in the body fluid and the dissolution of well crystallized HAp in the human body after implantation is too low to achieve optimum results in bioresorbility.

As the resorbability of a biomaterial depends principally on its dissolution rate,[9,10] which depends on microstructure (phase assemblage, porosity, surface roughness, etc.) conditioning the mechanical performance of implanted materials in the body, the understanding and the control of these parameters must be taken into serious account. Therefore, due to the complexity of calcium phosphate based biomaterials, further optimization of these materials is still required nowadays. For this reason,

* Corresponding author. Tel.: +34 917355840; fax: +34 917355843.
E-mail address: leticia.carbajal@icv.csic.es (L. Carbajal).

0955-2219/$ – see front matter © 2011 Elsevier Ltd. All rights reserved.
doi:10.1016/j.jeurceramsoc.2011.09.025

Table 1
Main characteristics of the reagents used for the synthesis of pure and Zn tricalcium phosphate based materials.

Raw materials	Purity (%)	$\rho^{25\,°C}$ (g/cm^3)	d_{50} (μm) as received	d_{50} (μm) optimized	S_e (m^2/g)
$NH_4H_2PO_4$ Fluka	≥99.0	1.80	427.5	28.4	0.02
$CaCO_3$ Panreac	99.0	2.61	16.7	16.7	0.11
ZnO Oxizinc-Agalsa	99.9	5.49	1.0	1.0	6.50

in the last decades, a new approach has been considered in order to optimize synthesis, phase compatibility, microstructure, dissolution rate, mechanical resistance and osteogenesis of tricalcium phosphate based biomaterials enhancing not only bone formation but also tissue regeneration. It consists in doping TCP with trace elements which do not break biocompatibility. Some of the chemical components which can be used as additives: CO_3^{2-}, SiO_4^{2-}, Mg^{2+}, Zn^{2+}, F^-, Cl^-, Na^+ and K^+, are restricted to elements contained in natural bone.[11,12] As the zinc content observed in human bone ranges from 0.0126 to 0.0217 wt%, zinc is suggested in several studies[13–16] and is of particular interest because it is an essential trace element that stimulates bone growth and their mineralization.[17] β-TCP (low temperature polymorph) is a potential zinc carrier[18–20] that can incorporate divalent cations with an ionic radius ranging from 0.060 to 0.080 nm, which is the case of Zn^{2+} (0.075 nm) decreasing its solubility "*in vitro*".[21] Zinc has been demonstrated to have a variety of roles in the mammalian system being essential for growth in human and many animals, associating a zinc deficiency with bone growth retardation.[22,23] Zn deficiency has been associated not only with skeletal growth retardation but also with premenopausal bone mass and postmenopausal osteoporosis.[24,25] Clinical trials have also shown that Zn supplementation inhibits postmenopausal bone loss[26] and osteoclastic bone resorption *in vitro*.[27] However, zinc must be released slowly from the implant because at an elevated level it can induce adverse reactions.[14]

In this context, the control of β/α-TCP phase ratio and assemblage, chemically modified with ZnO on the final implant will be interesting, allowing the development of biphasic Zn-TCP based materials with an enhanced combination of "*in vivo*" structural, mechanical and dissolution performances of both phases. For this reason, the main purpose of this study was to develop zinc doped monophasic and biphasic β/α-TCP biomaterials with different ZnO contents and different phase proportions of β/α polymorphs. The choice of the different Zn doped TCP stoichiometry compositions presented in this study was performed taking into account a previous research,[28] in which the isothermal section of ZnO–CaO–P_2O_5 ternary system at 900 °C was investigated. In particular the obtained data concerned to the phase compatibility regions and the solid solution extension region of Zn^{2+} in TCP in the rich tricalcium phosphate region of the system. This information was fundamental in order to design the zinc doped tricalcium phosphate based materials with tailored composition and microstructure considered in this research. The effect of ZnO content and sintering temperature on phase assemblage and microstructure has been investigated.

2. Experimental

Different TCP and zinc doped TCP ceramics were synthesized by conventional solid-state sintering process with a previous calcination step of the homogenized powders. The raw materials used in this study were ultra pure $NH_4H_2PO_4$ (≥99.0% – Fluka), $CaCO_3$ (99.0% – Panreac) and ZnO (99.9% – Oxizinc-Agalsa). Table 1 shows the main characteristics, average particle sizes, d_{50}, and specific surfaces of the raw materials selected in this research. As the as received precursors presented a wide dispersion of particle sizes, first of all $NH_4H_2PO_4$ was milled individually in an attrition-mill in isopropyl media using zirconia balls for 4 h in order to obtain an appropriate particle size distribution to optimize further synthesis. The average particle size, d_{50}, obtained after the milling step for $NH_4H_2PO_4$ was 28.4 μm, closer to the other reagents used.

Compositions, summarized in Table 2, with 0, 0.125, 0.250, 0.500 and 1.000 wt% ZnO doped TCP were prepared by mixing the proper amounts of the previously milled reagent powders in an attrition-mill using ZrO_2 balls in isopropyl media for 2 h. After the milling step, the powders were oven dried at 60 °C for 24 h, crushed and passed through a 63 μm sieve and calcined at 900 °C for 2 h. Subsequently the calcined stoichiometric powders were attrition milled again and sieved.

The stoichiometric powders before and after the calcined step were all thermal characterized by means of differential thermal and thermo-gravimetric analyses (DTA–TG) using a NETZSCH STA 409 analyzer in order to study the kinetics of phase transformation processes and chemical reaction mechanisms up to 1500 °C, with at a heating rate of 3 °C/min in a flowing air atmosphere. Particle size distribution and specific surface area of all the raw precursors and stoichiometric powders before and after the calcined step were evaluated by laser particle size analyzer Mastersizer Malvern Instruments in ethanol media and Monosorb Quanta Chrome, respectively.

The Fourier transform infrared spectrum (FT-IR) was recorded for all stoichiometric calcined powders in a

Table 2
Chemical composition of the different samples prepared.

Compositions	wt%			Ca/P ratio
	ZnO	CaO	P_2O_5	
TCP	–	54.235	45.765	1.50 ± 0.01
0.125 Z	0.125	54.128	45.747	1.50 ± 0.01
0.25 Z	0.250	54.021	45.729	1.50 ± 0.01
0.5 Z	0.500	53.806	45.694	1.50 ± 0.01
1.0 Z	1.000	53.378	45.622	1.50 ± 0.01

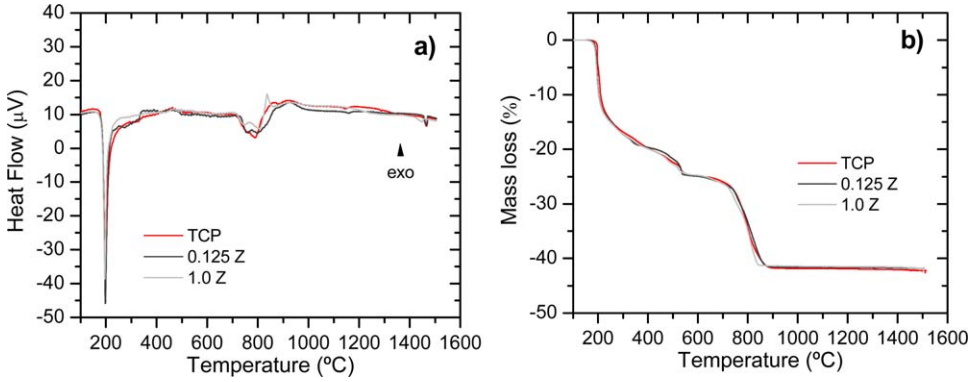

Fig. 1. (a) DTA and (b) TG curves obtained for stoichiometric mixtures of pure TCP, 0.125 Z and 1.0 Z before the calcined step.

Perkin-Elmer FTIR 1720X spectrometer using the KBr pellet technique. Briefly, a few milligrams of each sample were mixed with KBr in an agate mortar, pressed into disks, obtaining the different spectrum in the range of 4000–400 cm^{-1}. In order to identify the crystalline phases present in all the calcined powders, XRD patterns were performed (angular range: $2\theta = 10$–70, step scan = 0.0335) using a Vantec D8 Advance (Bruker).

Subsequently, calcined powders were isostatically pressed at 200 MPa into cylinders of 10 mm in diameter and 4 cm long and then cut into 10 mm diameter 2 mm thick disks. The pellets were sintered at a heating rate of 3 °C/min up to 1000, 1100 and 1250 °C in the case of pure TCP powders and 1150, 1200, and 1250 °C in the case of Zn-TCP powders for 12 h. Finally, the samples were cooled to 1000 °C at a rate of 50 °C/min and subsequently at a rate of 10 °C/min up to room temperature. The TCP and Zn doped TCP materials obtained were characterized in terms of compositional, structural and microstructural properties. Bulk density of the sintered samples was measured in water using the Archimedes method. Theoretical density was taken to be 3.07 g/cm^3 for β-TCP and 2.86 g/cm^3 for α-TCP. The X-ray diffraction patterns used to identify and quantify the crystalline phases present in all the sintered powdered samples were performed using an angular range: $2\theta = 10$–90, step scan = 0.0197. In order to quantify the different mineralogical phases present in the XRD patterns a "modified" internal pattern method[29] based on the one proposed by Klug and Alexander, and Chung[30–32] was carried out. This method was applied since it eliminates, through a rigorous mathematical artifice, the effect of the mass absorption coefficients performing a calibration curve. Compositions with 100β, 75β/25α, 50β/50α, 25β/75α and 100α (wt%) were obtained and used to establish the calibration curve. This method is a simple and high accuracy method of quantification between phases with similar mass absorption coefficients.

Additionally, for all thermal treated compositions higher than 900 °C, the Ca/P molar ratio was determined by inductively coupled plasma-optical emission spectroscopy (ICP-OES).

Microstructure was evaluated on polished and chemically etched with acetic acid samples using a Field Emission Scanning Electron Microscope, FE-SEM (Hitachi S-4700, Tokio, Japan), equipped with Energy Dispersive Spectroscopy (EDS). Porosity, grain size and phase proportion of the crystalline phases present was evaluated on polished and etched surfaces by using image processing and analysis program (Leica Qwin Pro, Leica Microsystems Imaging Solutions Ltd., Cambridge).

3. Results and discussion

3.1. Homogenized powder characterization

3.1.1. DTA–TG analyses

Fig. 1 shows the DTA–TG curves obtained for stoichiometric homogenized powders only in the case of pure TCP, 0.125 Z and 1.0 Z, recorded from room temperature up to 1500 °C at a heating rate of 3 °C/min, before the calcined step. DTA–TG curves were also recorded for the intermediate dopant content compositions; however as these results exhibit the same feature as the ones presented in Fig. 1, they were not shown in order to clarify the figure. According to the DTA curves recorded (Fig. 1a), three endothermic peaks were resolved up to 1500 °C in all the compositions. The first thermal event, associated with an endothermic peak at $T \sim 200$ °C and experimental weight loss of ∼13.5 wt%, according to the TG curves (Fig. 1b), can be attributed to the melting and partial decomposition of $NH_4H_2PO_4$ ($NH_4H_2PO_4 \leftrightarrow NH_3(g) + H_3PO_4(l)$), since XRD patterns performed at 250 °C show peaks attributed only to $CaCO_3$. The second thermal event was associated with a broad endothermic peak in the range $T \sim 715$–860 °C and experimental weight loss of ∼14.8 wt% (Fig. 1b). The XRD patterns performed at 700 °C and 860 °C (not shown), allowed the identification of the thermal processes taking place in this temperature range. At 700 °C peaks associated to $CaCO_3$ with decreased intensity compared to those obtained at 250 °C, peaks associated to β-$Ca(PO_3)_2$ and small peaks attributed to HAp were observed in the XRD patterns, which evidenced the partial decomposition of $CaCO_3$. In addition the XRD patterns performed at 860 °C confirmed the crystallization of β-TCP and the presence of a small amount of HAp and β-$Ca_2P_2O_7$. No evidence of peaks associated to $CaCO_3$ was observed at this temperature, this result was coincident with the total decomposition of the remaining $CaCO_3$ left. Only in the case of composition 1.0 Z (1.000 wt% ZnO) the crystallization of β-TCP can be associated with a small exothermic peak at 836 °C which suggested that the ZnO content in the compositions tends to activate the β-TCP crystallization.

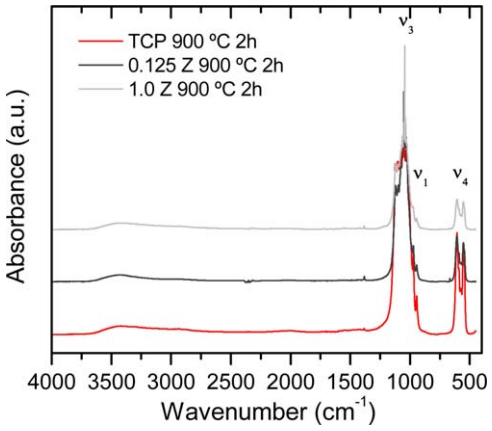

Fig. 2. FT-IR spectrum obtained for pure TCP, 0.125 Z and 1.0 Z calcined at 900 °C for 2 h.

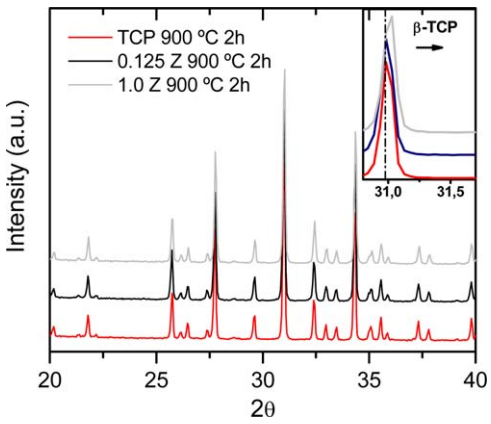

Fig. 3. XRD patterns obtained for pure TCP, 0.125 Z and 1.0 Z calcined at 900 °C for 2 h.

Finally the third endothermic peak observed between $T \sim 1440$ and 1467 °C, depending on the composition, was attributed to the TCP polymorphic $\alpha \rightarrow \alpha'$ transformation.

The samples exhibited a total experimental weight loss between 41.70% and 41.30% upon heating to 900 °C (Fig. 1b) which corresponded with TCP up to 1.0 Z composition. This result evidenced how the experimental mass loss decreased slightly with the increasing ZnO content in the composition. The theoretical values due to the evolution of the gaseous species (H_2O, NH_3 and CO_2) were calculated for each composition: TCP, 0.125 Z and 1.0 Z to be 41.50%, 41.48% and 41.25%, respectively. The total experimental mass losses obtained in the TG curves fitted with the theoretical values predicted.

It is possible to make a distinction between five different thermal events associated with five weight losses up to 1500 °C in all the compositions which were in accordance with a previous research.[33] However, only two were associated in DTA curves with the two endothermic peaks previously commented. This puts into evidence that the different processes, during the reaction path to β-TCP, take place sequentially. This is the case of $CaCO_3$ decomposition (250–860 °C) and the formation of β-$Ca(PO_3)_2$, HAp, β-$Ca_2P_2O_7$ intermediate compounds.

Finally, from all this information what could be gathered from the DTA–TG analyses was that at temperatures above 900 °C, the elimination of H_2O, NH_3 and CO_2 was completed in all the homogenized powder samples.

3.2. Calcined powder characterization

Taking into account the DTA–TG results obtained in Section 3.1.1, the appropriate calcination treatment selected previous to the future synthesis of the biomaterials in this study, was 900 °C held for 2 h. As in Section 3.1, all the calcined compositions were studied however only the data concerned to pure TCP, 0.125 Z and 1.0 Z were shown in Figs. 2–4.

3.2.1. FT-IR analyses

In order to ensure the accuracy of the calcined treatment carried out, FT-IR spectrum in the absorbance configuration in the case of pure TCP, 0.125 Z and 1.0 Z calcined at 900 °C for 2 h were shown in Fig. 2. From the obtained results it can be gathered that the main normal vibration modes observed in all the compositions were associated to the PO_4^{3-} ion.[34,35] The peak observed around 940 cm^{-1} corresponds to the non-degenerate P–O symmetric stretching mode ν_1. The bands at 553 and 605 cm^{-1} were attributed to the triply degenerate bending mode ν_4 and the band at ~420 cm^{-1} to the double degenerate bending mode ν_2 which correspond to the bending vibrations of the O–P–O bond. Besides, the band associated to the triply degenerate asymmetric P–O stretching mode ν_3 was observed in the range 962–1062 cm^{-1}. The absence of peaks associated to vibration modes linked to NH_4^+ and CO_3^{2-} ions enhances the effectiveness of the calcined treatment chosen in this study.

3.2.2. XRD analyses

The XRD patterns recorded in the case of calcined pure TCP, 0.125 Z and 1.0 Z compositions were displayed in Fig. 3. Well crystallized peaks associated to β-TCP were observed in all the compositions. The absence of diffraction peaks associated to ZnO and the small displacement observed in β-TCP main diffraction peak represented in the inset of Fig. 3 confirmed the incorporation of Zn^{2+} into β-TCP structure, studied in more detail in a previous research.[19,28]

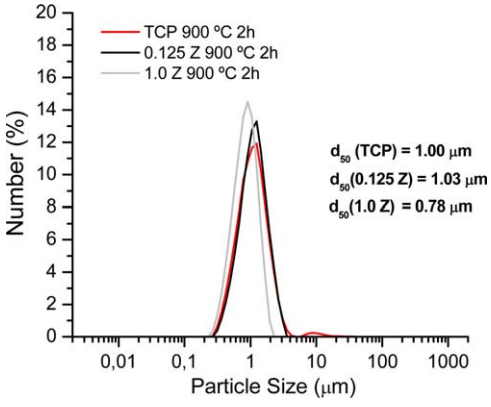

Fig. 4. Particle size distribution obtained for pure TCP, 0.125 Z and 1.0 Z powders calcined at 900 °C for 2 h.

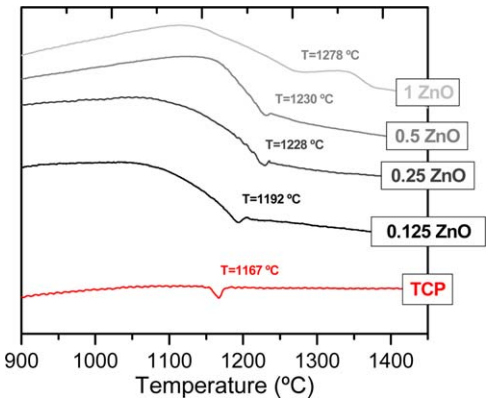

Fig. 5. DTA curves (between 900 and 1450 °C) of TCP and Zn-TCP compositions calcined at 900 °C for 12 h.

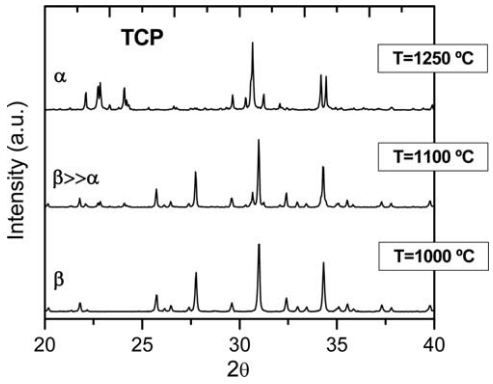

Fig. 6. XRD patterns obtained for pure TCP up to 1000, 1100 and 1250 °C for 12 h.

3.2.3. Chemical analyses

The Ca/P molar ratio of all thermal treated compositions higher than 900 °C was determined by ICP-OES to be 1.50 ± 0.01.

3.2.4. Particle size distribution and specific surface area

The particle size distribution was measured and represented, Fig. 4, in the case of pure TCP, 0.125 Z and 1.0 Z calcined powders. A very narrow particle size distribution, reducing in one order of magnitude the d_{50} of the calcined powders when compared to the optimized ones (Table 1), was obtained in all powders previous to the sintering step. Close values of the specific surface area of 7.0 m^2/g, 7.5 m^2/g and 6.4 m^2/g were obtained for calcined pure TCP, 0.125 Z and 1.0 Z powders, respectively. These results were considered valuable for good sinterability.

3.2.5. DTA–TG analyses

To analyze the kinetics of phase transformation processes of β/α-TCP polymorphs as a function of the ZnO content, a different calcination treatment was carried out in all the stoichiometric homogenized compositions (Table 2). In this case the temperature was kept to be 900 °C, but it was held up to 12 h in order to ensure well crystallized β-TCP phase in all the primary calcined powders.

Fig. 5 shows the DTA curves of pure TCP and all Zn-TCP powders calcined at 900 °C for 12 h, recorded from room temperature up to 1450 °C at a heating rate of 3 °C/min. One endothermic peak was observed in all DTA curves. This endothermic peak was attributed to the β → α transformation.

According to the literature[36,37] the β → α transformation takes place in the temperature range which goes from 1125 to 1200 °C. In our case for pure TCP the rapid and reversible endothermic transformation β → α takes place at 1167 °C. For the rest of the compositions we can see how this transformation shifts to higher temperatures, from 1192 °C up to 1278 °C, with the increasing ZnO content. Additionally, it is also evident that this endothermic event was progressively inhibited when the ZnO content increases in the compositions, in particular in the case of 1.0 Z, obtaining a smoother DTA curve leading to an important inhibition of the transformation. This shift observed in the polymorph transformation up to higher temperatures puts into evidence the stabilizing effect of zinc on the β-TCP phase structure.[38]

3.3. Material characterization

Pure TCP and Zn-TCP materials were sintered by solid state sintering reaction from the previously calcined stiochiometric powders. Samples were sintered at 1000, 1100 and 1250 °C in the case of pure TCP and at 1150, 1200 and 1250 °C in the case of Zn-TCP compositions. Subsequently they were characterized in terms of structural and microstructural evolution.

3.3.1. XRD analyses

Fig. 6 shows the XRD patterns recorded for pure TCP sintered at three different temperatures for 12 h. At 1000 °C only

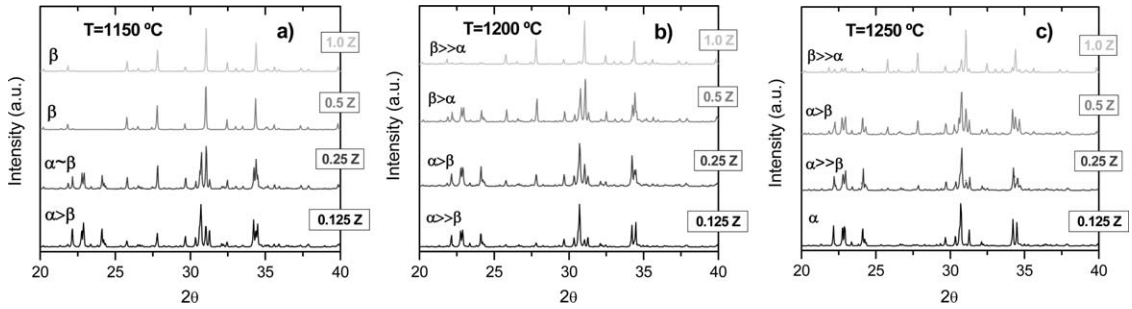

Fig. 7. Compared XRD patterns obtained for the different Zn-TCP compositions sintered up to: (a) 1150 °C, (b) 1200 °C and (c) 1250 °C for 12 h.

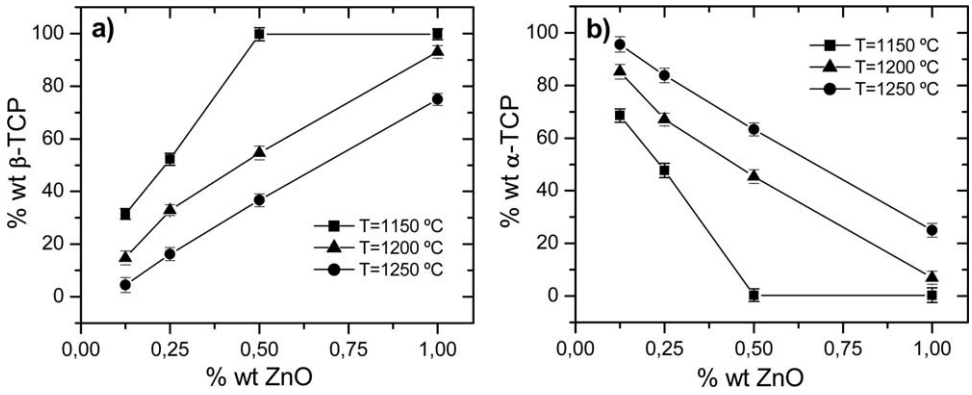

Fig. 8. Quantification of (a) β and (b) α-TCP polymorphs in each sintered Zn-TCP material as function of ZnO content and sintering temperature.

diffraction peaks attributed to β-TCP were observed. When the sintering temperature increased up to 1100 °C, we clearly observed that β-TCP phase had already begun to transform into α-TCP obtaining diffraction peaks attributed to both phases. This transformation was fully completed when the sintering temperature of 1250 °C was reached, obtaining peaks exclusively associated to α-TCP polymorph.

The collection of the XRD patterns obtained for all the Zn-TCP compositions sintered at 1150, 1200 and 1250 °C for 12 h was illustrated in Fig. 7. A comparative XRD study within the different zinc content in each composition versus the sintering temperature is displayed in Fig. 7(a)–(c). As a whole, these results give a very illustrative and complete mapping of all the different possible microstructure material configurations (Zn doped α-TCP, Zn doped β-TCP or Zn doped biphasic α/β-TCP) attending to phase assemblage, zinc content and sintering temperature when designing Zn-TCP based biomaterials in the future. In addition the phase proportions of both polymorphs as function of ZnO content for each sintering temperature has been quantified from the XRD patterns previously obtained using a "modified" internal pattern method.[29]

Fig. 8 shows the wt% β-TCP and wt% α-TCP phases as function of the wt% ZnO content in each composition and for each temperature. In Fig. 8a, we can clearly observe how the β-TCP phase proportion is increasing with the increase ZnO content in the composition when we keep constant the sintering temperature and decreases with the increase of the sintering temperature for constant ZnO content. The opposite behavior is observed for α-TCP (Fig. 8b).

From these results the main conclusion we can extract was that the incorporation of zinc in TCP structure is stabilizing β-TCP phase up to higher temperatures. Consequently we are able to obtain zinc doped β-TCP based materials nearly up to 1200 °C when we incorporate 1 wt% ZnO. This result is in accordance with the previous reported data obtained in the DTA analyses.

3.3.2. Densification

The effect of the sintering temperature and the ZnO content on the densification of pure and ZnO doped β/α-TCP based materials has also been assessed. Fig. 9 shows the densification of each sintered composition as a function of temperature. In the case of pure TCP (Fig. 9a), the densification increases from 75% up to 90% in the temperature range of 1000–1100 °C and then decreases up to 82% at 1250 °C. This last remarkable decrease in the densification was attributed to the complete transformation of β-TCP into α-TCP polymorph in pure TCP, which is a less dense phase than β-TCP. The total porosity achieved in pure TCP based materials varied in the range 10–25%.

In the case of the Zn-TCP compositions (Fig. 9b) two effects were observed. There was an initial decrease of the densification with the sintering temperature up to 1200 °C in most of the samples, due to the increase of the α-TCP proportion in the compositions. Although α-TCP phase proportion continued to increase with temperature up to 1250 °C, according to the

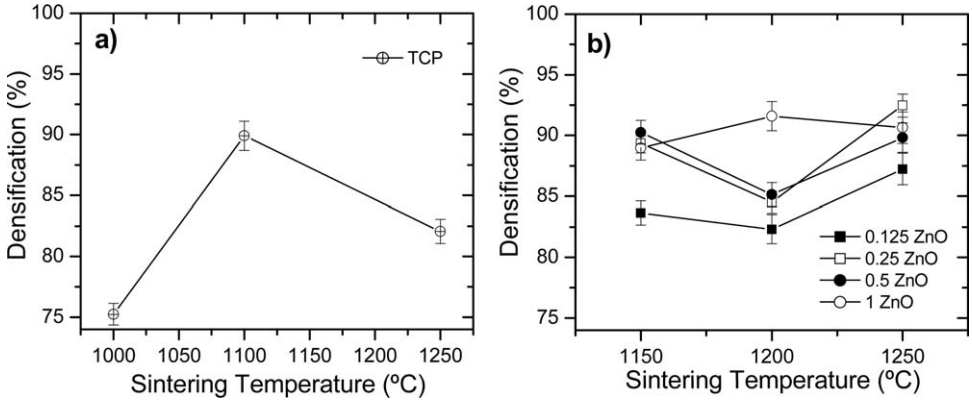

Fig. 9. Densification of (a) pure TCP and (b) Zn-TCP compositions versus the sintering temperature.

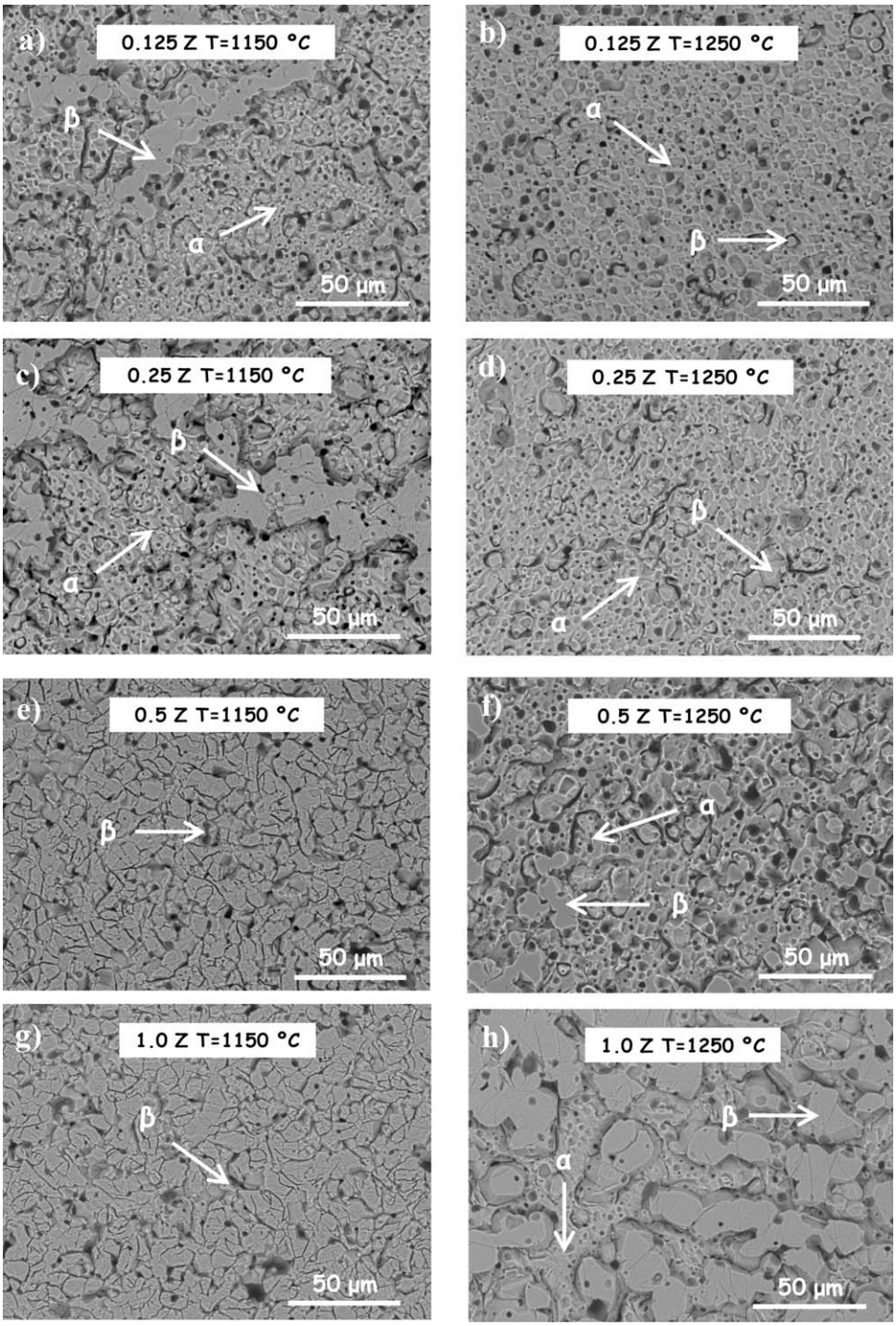

Fig. 10. FE-SEM images of different Zn-TCP compositions: (a), (c), (e) and (g) sintered at 1150 °C and (b), (d), (f) and (h) sintered at 1250 °C.

XRD patterns previously commented the higher densification achieved for most compositions may be due to the increase of the sintering temperature which was the driving force enhancing sinterability up to 1250 °C. In these cases the theoretical density percentage increased around 5–8% in the temperature range from 1200 to 1250 °C. Only in the case of sample 1.0 Z we observed some differences, as the densification increases up to 1200 °C and then slightly decreased. This behavior can be explained taking into account that the small increase of α-TCP phase proportion (∼7%) up to 1200 °C, was not sensitive enough to produce a shift in the densification curve, being the sintering temperature the dominant effect in this case. Contrary, up to 1250 °C the almost horizontal slope observed in the densification curve evidenced that both effects contributing were more or less balanced. The total porosity achieved in Zn-TCP based varied in the range 8–17%.

3.3.3. Microstructural evolution

In order to carry out the microstructural assessment of the sintered obtained materials, the samples were previously chemically etched with diluted acetic acid (1:9) for 30 s. Fig. 10 shows the chemically etched FE-SEM images collected of all zinc doped TCP compositions sintered at 1150 °C and 1250 °C for 12 h.

In the case of 0.125 Z and 0.25 Z compositions (ZnO content ≤0.250 wt%) sintered at 1150 °C (Fig. 10a and c), the presence of two different phases in the microstructures can be observed in the micrographs. The β/α phase proportion quantifications obtained from the XRD patterns, allowed the identification of these two phases, which were pointed out in the micrographs for better clarity. The smother and coarse phase, less susceptible to the chemical attack, was attributed to β-TCP whereas the much rougher and rounded phase higher susceptible to the etching process carried out corresponded to α-TCP. In both cases α-TCP comprises the matrix of the material, whose morphology is composed of quasi-equiaxial grains homogenously distributed, being smaller (∼5–10 μm) than those of β-TCP (∼10–15 μm). Contrary, the disposition of the β-TCP crystals within the microstructure, constitute some kind of elongated aggregates. According to 0.5 Z and 1.0 Z compositions (ZnO content ≥0.500 wt%) also sintered at 1150 °C (Fig. 10e and g), monophasic microstructures constituted of a homogenous and continuous matrix of β-TCP crystals (≤10 μm), were observed in both cases. The crystals and the grain boundaries appear to be well defined within the etching process carried out. Finally, a slight decrease of the grain size of β-TCP phase as the dopant content increases in the range 0.250–0.500 wt% ZnO at 1150 °C, can be gathered from the image analyses performed on the collection of the micrographs recorded.

In a similar way, in the case of the materials sintered at 1250 °C for 12 h, compositions 0.125 Z and 0.25 Z (ZnO content ≤0.250 wt%) exhibit similar textures composed of a majority α-TCP matrix (Fig. 10b and d). Moreover, some scarce and isolated crystal nucleation of β-TCP crystals observed in a higher proportion in composition 0.25 Z (17%) when compared to composition 0.125 Z (5%), embedded in the α-TCP matrix can be noticed (Fig. 10d). Furthermore, in compositions 0.5 Z and 1.0 Z (ZnO contents ≥0.500 wt%) a biphasic configuration is evident from the microstructures. The α-TCP phase still constitutes the continuous matrix in the micrographs. The main difference observed when compared to the lower dopant content microstructures sintered at 1250 °C, is the important increase in the amount of β-TCP phase and the grain growth of β-TCP grains with the increasing ZnO content. In the case of 1.0 Z (Fig. 10h), they constituted the same elongated arrangement observed at low temperature (0.125 Z and 0.25 Z at 1150 °C) sintered materials. The increase in the grain size is more evident in 1.0 Z composition obtaining a mean grain size of ∼20 μm.

According to the phase assemblage of the biphasic β/α-TCP microstructure configurations obtained in the case of the 0.125 Z and 0.25 Z sintered materials at 1150 °C (Fig. 10a and c) compared to the ones achieved for compositions 0.5 Z and 1.0 Z sintered at 1250 °C (Fig. 10f and h), it can be gathered that β-TCP phase appears to be considerably more homogenously distributed at 1250 °C than at 1150 °C. For almost equal phase proportions of β/α-TCP polymorphs, obtained in 0.125 Z, T = 1150 °C (Fig. 10a) and 0.5 Z, T = 1250 °C (Fig. 10f), the β-TCP phase distribution in the material is clearly more homogenous in the case of the highest dopant percentage. In addition, from the biphasic microstructural material configurations, it can be extracted that the Zinc may be involved in topotactic transformation, acting as an inhibitor during the β → α transformation. This fact could be related to the crystal structure of β-TCP,[39,40] which has a rhombohedral structure (space group $R3c$), that can be described by A and B columns running along the c axis. Previously,[18,19] it has been described how this structure can incorporate lower sized Zn^{2+} (0.075 nm) at the higher sized Ca^{2+} sites, occupying preferentially the Ca(5) sites in β-$Ca_3(PO_4)_2$ structure. As the ZnO content increases in the compositions, more Ca(5) positions were occupied in the A columns of β-TCP crystal structure. This will motivate a wider and more homogenous distribution of Zn^{2+} in β-TCP structure, retaining this phase in more areas of the microstructure up to higher temperatures, until the total transformation to α-TCP phase takes place.

Consequently, from the results obtained in this section, it can be gathered that the control of the ZnO dopant content and the sintering temperature allows the development of different microstructural material configurations attending to β/α-TCP phase assemblage and proportions. This result is very interesting from the viewpoint of the development of tailored biomaterials for future hard tissue replacement demand applications.

4. Conclusions

TCP and Zn doped TCP dense based biomaterials were synthesized by two step solid-state sintering process.

The effect of ZnO on the β → α tricalcium phosphate polymorphic transformations has been established. The increasing in the polymorphic transformation temperature β → α TCP is result of the stabilizing effect of Zn^{2+} on the β-TCP structure, in which thermal stability of β-TCP phase ranged from 1167 °C in the case of pure TCP up to 1278 °C in the case 1.000 wt% ZnO doped TCP.

The tailoring of the microstructure phase assemblage with different β/α-TCP polymorphs configurations can be gathered, just by modulating the sintering temperature and the ZnO content in the compositions. This result allowed the design of β-TCP monophase bioceramics and biphasic β/α-TCP bioceramics at 1150 °C and 1250 °C respectively with improved densification.

Acknowledgements

L. Carbajal acknowledges project CICYT MAT2007-65857 and BES-2008-004317 for financial support.

The authors will like to dedicate this manuscript to the memory Prof. Salvador De Aza.

References

1. Hench LL. Bioceramics: from concept to clinic. *J Am Ceram Soc* 1991;**74**(7):1487–510.

2. Putlyaev VI, Safronova TV. A new generation of calcium phosphate biomaterials: the role of phase and chemical compositions. *Glass Ceram* 2006;**63**:3–4.
3. Kokubo T. Bioceramics and their clinical applications. In: Kokubo T, editor. *Japan medical materials*. 2008.
4. Hench LL, Wilson J. *An introduction to bioceramics*. London, UK: World Scientific; 1993.
5. Fernandez E, Gil FJ, Ginebra MP, Diessens FCM, Planell JA. Calcium phosphate bone cements for clinical applications. Part I. Solution chemistry. *J Mater Sci: Mater Med* 1999;**10**:169–76.
6. Kwon SH, Jun YK, Hong SH, Lee IS, Kim HE, Won YY. Calcium phosphate bioceramics with various porosites and dissolution rates. *J Am Ceram Soc* 2002;**85**(12):3129–31.
7. Suzuki T, Yamamoto T, Toriyama M, et al. Surface instability of calcium phosphate ceramics in tissue culture medium and the effect on adhesion and growth of anchorage-dependent animal cells. *J Biomed Mater Res* 1997;**34**:507–17.
8. Yamada S, Heymann D, Bouler J-M, Daculsi G. Osteoclastic resorption of calcium phosphate ceramics with different hydroxyapatite/β-tricalcium phosphate ratios. *Biomaterials* 1997;**18**:1037–41.
9. Sainz MA, Pena P, Serena S, Caballero A. Influence of design on bioactivity of novel $CaSiO_3$–$CaMg(SiO_3)_2$ bioceramics: in vitro simulated body fluid test and thermodynamic simulation. *Acta Biomater* 2010;**6**(7):2797–807.
10. Hoppe A, Nusret SG, Boccaccini AR. A review of the biological response to ionic dissolution products from bioactive glasses and glass–ceramics. *Biomaterials* 2011;**32**:2757–74.
11. Carrodeguas RG, De Aza AH, García-Paéz I, De Aza S, Pena P. Revisiting the phase-equilibrium diagram of the $Ca_3(PO_4)_2$–$CaMg(SiO_3)_2$ system. *J Am Ceram Soc* 2010;**93**(2):561–9.
12. Douard N, Detsch R, Chotard-Ghodsnia R, Damia C, Deisinger U, Champion E. Processing, physico-chemical characterisation and in vitro evaluation of silicon containing β-tricalcium phosphate ceramics. *Mater Sci Eng C* 2011;**31**:531–9.
13. Ito A, Kawamura H, Otsuka M, et al. Zinc-releasing calcium phosphate for stimulating bone formation. *Mater Sci Eng C* 2002;**22**:21–5.
14. Ito A. Preparation, solubility and cytocompatibility of zinc-releasing calcium phosphate ceramics. *J Biomed Mater Res* 2000;**50**:178–83.
15. Cuneyt Tas A, Sarit B, Bhaduri SB, Jalota S. Preparation of Zn-doped β-tricalcium phosphate (β-$Ca_3(PO_4)_2$) bioceramics. *Mater Sci Eng C* 2007;**27**(3):394–401.
16. Bandyopadhyay A, Withey EA, Moore J, Bose S. Influence of ZnO doping in calcium phosphate ceramics. *Mater Sci Eng C* 2007;**27**:14–7.
17. Wei X, Akinc M. Si, Zn-modified tricalcium phosphates: a phase composition and crystal structure study. *Key Eng Mater* 2005;**284–286**:83–6.
18. Bigi A, Foresti E, Gandolfi M, Gazzano M, Roveri N. Isomorphous substitutions in β-tricalcium phosphate: the different effects of zinc and strontium. *J Inorg Biochem* 1995;**66**:259–65.
19. Kannan S, Goetz-Neunhoeffer F, Neubauer J, Ferreira JMF. Synthesis and structure refinement of zinc-doped β-tricalcium phosphate powders. *J Am Ceram Soc* 2009;**92**(7):1592–5.
20. Wei X, Akinc M. Crystal structure analysis of Si and Zn Co doped tricalcium phosphate by neutron powder diffraction. *J Am Ceram Soc* 2007;**90**(9):2709–15.
21. Ito A. Resorbability and solubility of zinc-containing tricalcium phosphate. *J Biomed Mater Res* 2002;**60**:224–31.
22. Yamaguchi M, Yamaguchi R. Action of zinc on bone metabolism in rats. Increases in alkaline phosphatase activity and DNA content. *Biochem Pharmacol* 1986;**35**(5):773–7.
23. Yamaguchi M, Oishi H, Suketa Y. Stimulatory effect of zinc on bone formation in tissue culture. *Biochem Pharmacol* 1987;**3622**:4007–12.
24. Hertzberg M, Foldes J, Steinberg R, Menczel J. Zinc excretion in osteoporotic women. *J Bone Miner Res* 1990;**5**:251–7.
25. Angus RM, Sambrook PN, Pocock NA, Eisman JA. Dietary intake and bone mineral density. *J Bone Miner Res* 1988;**4**(3):265–77.
26. Saltman PD, Strause LG. The role of trace minerals in osteoporosis. *J Am Coll Nutr* 1993;**12**(4):384–9.
27. Moonga BS, Dempster DW. Zinc is a potent inhibitor of osteoclastic bone resorption in vitro. *J Bone Miner Res* 1995;**10**(3):453–7.
28. Carbajal L, Sainz MA, Serena S, Caballero AC, Caballero A. Solid-state compatibility in two regions of the system ZnO–CaO–P_2O_5. *J Am Ceram Soc* 2011;**94**(7):2213–9.
29. Bartolomé JF. Análisis Mineralógico cuantitativo por difracción de rayos X, Aplicación del método del patrón interno "modificado" en el estudio de compuestos de Al_2O_3–Al_2TiO_5. *Bol Soc Esp Cerám y Vidrio* 1996;**35**(4):271–83.
30. Klug HP, Alexander LE. X-ray diffraction procedures. In: *2nd ed.*. New York: John Willey and Sons; 1974.
31. Chung FH. Quantitative interpretation of X-ray diffraction patterns of mixtures. I. Matrix-flushing method for quantitative multicomponent analysis. *J Appl Cryst* 1974;**7**:519.
32. Chung FH. Quantitative interpretation of X-ray diffraction patterns of mixtures. II. Adiabatic principle of X-ray diffraction analysis of mixtures. *J Appl Cryst* 1974;**7**:526.
33. TenHuisen KS, Brown PW. Phase evolution during the formation of α-tricalcium phosphate. *J Am Ceram Soc* 1999;**82**(10):2813–8.
34. Jillavenkatesa A, Condrate RA. The infrared and Raman spectra of β and α tricalcium phosphate $Ca_3(PO_4)_2$. *Spectrosc Lett* 1998;**31**(8):1619–34.
35. Vani R, Girija K, Elayaraja K, Prakash Parthiban S, Kesavamoorthy R, Narayana Kalkura S. Hydrothermal synthesis of porous triphasic hydroxyapatite (α and β) tricalcium phosphate. *J Mater Sci: Mater Med* 2009;**20**:S43–8.
36. Welch JH, Gutt W. High-temperature studies of the system calcium oxide–phosphorus pentoxide. *J Chem Soc* 1961:4442–4.
37. Serena S, Carbajal L, Sainz MA, Caballero A. Thermodynamic assessment of the system CaO–P_2O_5: application of the ionic two sublattice model to glass forming melts. *J Am Ceram Soc*. doi:10.1111/j.1551-2916.2010.04834.x.
38. Kreidler ER, Hummel FA. Phase equilibria in the system $Ca_3(PO_4)_2$–$Zn_3(PO_4)_2$. *Inorg Chem* 1967;**6**(3):524–8.
39. Yoshida K, Hyuga H, Kondo N, Kita H, Sasaki M, Mitamura M, Hashimoto K, Toda Y. Substitution model of monovalent (Li, Na, and K), divalent (Mg), and trivalent (Al) metal ions for β-tricalcium phosphate. *J Am Ceram Soc* 2006;**89**(2):688–90.
40. Yashima M, Sakai A, Kamiyama T, Hoshikawa A. Crystal structure analysis of β-tricalcium phosphate $Ca_3(PO_4)_2$ by neutron powder diffraction. *J Solid State Chem* 2003;**175**:272–7.